Observation of charge accumulation and onsite Coulomb repulsion at transition metal impurities in the iron pnictides

R. Kraus,[1] V. Bisogni,[1] L. Harnagea,[1] S. Aswartham,[1] S. Wurmehl,[1] G. Levy,[2] I. S. Elfimov,[2] B. Büchner,[1,3] G. A. Sawatzky,[2] and J. Geck[1,*]

[1]*Leibniz Institute for Solid State and Materials Research, Helmholtzstrasse 20, D-01171 Dresden, Germany*

[2]*Department of Physics and Astronomy, University of British Columbia, 6224 Agricultural Road, British Columbia V6T 1Z1, Vancouver, Canada*

[3]*Institute for Solid State Physics, Dresden Technical University, TU-Dresden, 01062 Dresden, Germany*

(Received 30 April 2012; revised manuscript received 11 April 2013; published 24 April 2013)

We report a combined valence band photoemission and Auger spectroscopy study of single crystalline $Ca(Fe,Co)_2As_2$ and $Ba(Fe,TM)_2As_2$ with transition metal TM = Ni or Cu. The valence band photoemission data show directly that the TM states move to higher binding energies with increasing atomic number, contributing less and less to the states close to the Fermi level. Furthermore, the $3d^8$ final state of the LVV Auger decay, which is observed for Ni and Cu, unambiguously reveals the accumulation of charge at these impurities. We also show that the onsite Coulomb interaction on the impurity strongly increases when moving from Co over Ni to Cu. Our results quantify the impurity potentials and imply that the superconducting state is rather robust against impurity scattering.

DOI: 10.1103/PhysRevB.87.134516 PACS number(s): 74.70.Xa, 71.20.−b, 79.60.−i, 82.80.Pv

I. INTRODUCTION

High-temperature superconductivity (HTS) in the iron pnictides is one of the most intensively studied topics in current condensed matter science. Although research efforts established many properties of these materials, important questions still remain to be clarified.[1] One of these questions regards the effect of replacing a few percent of Fe by other transition metals (TMs) such as Co, Ni, or Cu. The substitution of Fe by Co or Ni induces HTS[2] and therefore it is very important to understand the effects of the TM impurities on the electronic structure. Exactly what these effects are, however, remains controversial (e.g., Refs. 3 and 4 and references therein).

It is often assumed that Co, Ni, and Cu mainly dope electrons into the Fe bands without seriously affecting the electronic structure otherwise.[5] But this interpretation has been challenged recently. While some studies confirm that the TM substitutions indeed dope additional charge carriers into the Fe bands,[6–8] others report the lack of additional charge at the Fe sites,[9–11] casting doubts on the electron doping via TM substitution. In addition, recent theoretical studies show that the random scattering potential introduced by the substituted TMs has important effects, which are often neglected but may in fact cause significant modifications to the electronic system.[2,3,12,13] The notion that the effects of TM substitution can go well beyond a mere charge doping is also supported by a recent angle-resolved photoemission study.[14] In what follows we will therefore discriminate between the term "doping", which refers to changing the number of charge carriers in the Fe:3d bands, and the substitution of Fe by other TMs.

The above shows that there is evidence that the effect of TM substitution on the electronic structure of the iron pnictides can be quite complex. But notwithstanding these recent developments, the role of TM substitution remains a matter of debate. In this paper, we shed light on this issue by means of photoemission spectroscopy (PES), Auger electron spectroscopy (AES), as well as model calculations. Specifically we report studies of $Ca(Fe,Co)_2As_2$ and $Ba(Fe,TM)_2As_2$ (TM = Ni, Cu). For Co we chose the Ca instead of the Ba material, in order to avoid complications due to the overlap of the Ba $M_{4,5}$ and the Co $L_{2,3}$ edges.[4] For all three systems we quantify the TM-impurity potentials and the corresponding onsite Coulomb interactions, which both depend strongly on the substituted TM element. We also directly observe the accumulation of charge at the substituted Ni and Cu sites. Our results underpin and clarify the nontrivial effects of TM substitution on the electronic structure of the iron pnictides.

II. EXPERIMENT

The experimental data were collected at the UE52-PGM beamline of the HZB-BESSY II synchrotron source. Single crystalline samples were grown as described elsewhere[15,16] and cleaved *in situ* just before the measurements, which resulted in fresh and mirror-like surfaces. More details about the sample growth and characterization can be found in the Appendix. PES and AES spectra were recorded using a Scienta R4000 hemispherical analyzer, whereas the x-ray absorption spectroscopy (XAS) spectra were measured via the total electron and fluorescence yield. The photon energy was calibrated against the Au 4f lines, which means that the measured binding energies always refer to the chemical potential. All spectra where recorded with the photon beam at an incident angle of 35° with respect to the sample surface, which was parallel to the FeAs layers. For the PES and AES measurements horizontal and vertical polarized light was used, respectively, to optimize the relative intensities of the two components.[17]

III. RESULTS

Soft x-ray valence band photoemission data for $Ca(Fe,Co)_2As_2$ and $Ba(Fe,TM)_2As_2$ (TM = Ni, Cu) are presented in Fig. 1, including the spectra of the corresponding pure parent compounds. In the case of the parent materials,

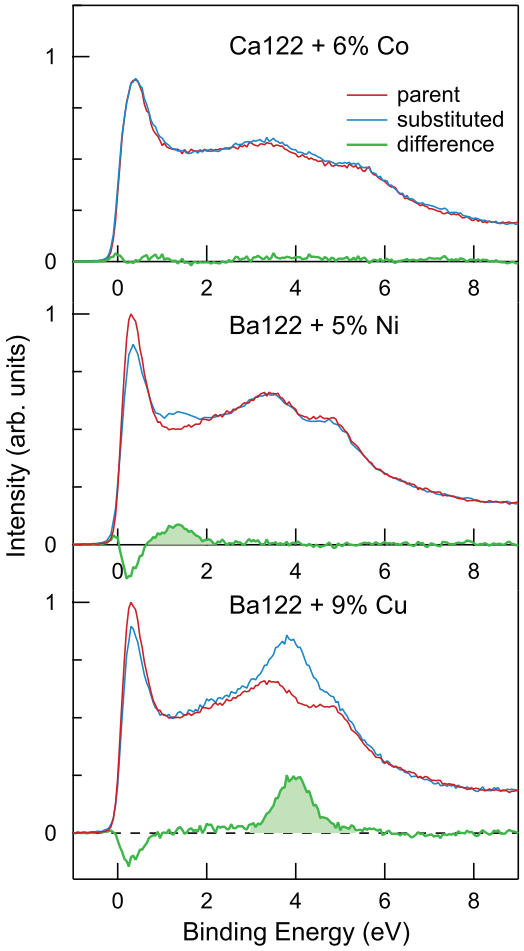

FIG. 1. (Color online) Valence band photoemission data for $BaFe_2As_2$, $CaFe_2As_2$, $Ca(Fe_{1-x}Co_x)_2As_2$ with $x = 0.06$, $Ba(Fe_{1-x}Ni_x)_2As_2$ with $x = 0.05$, and $Ba(Fe_{1-x}Cu_x)_2As_2$ with $x = 0.09$. All measurements were performed at room temperature using a photon energy of $h\nu = 600$ eV and normalized by the area above of 7 eV binding energy.

the PES intensity at 0–2 eV and 3–6 eV is due to mostly Fe:3*d* and As:4*p* derived bands.[18,19] The comparison of $Ca(Fe_{1-x}Co_x)_2As_2$ with $x = 0.06$ to its parent compound $CaFe_2As_2$, reveals that both spectra are identical within the error of the experiment. However, for the Ni- and Cu-substituted materials, additional features can be observed clearly in the valence band photoemission. An additional structure centered at the binding energy $\langle\epsilon_B^{\mathrm{Ni}}\rangle = 1.4$ eV is present in the Ni-substituted $BaFe_2As_2$, which does not exist in the parent material and which is evident in the difference of the two spectra. Even more striking, a strong additional peak at $\langle\epsilon_B^{\mathrm{Cu}}\rangle = 4$ eV is found for the Cu-substituted material. We stress that these additional features were fully reproducible and observed for different samples.

The PES data in Fig. 1 is experimental proof that the 3*d* impurity states move to higher binding energy with increasing atomic number *Z*. While the Ni states around 1.4 eV are still located inside the Fe bands, although close to the band bottom, the Cu impurity states are well below the Fe bands. The lack of additional features for the Co-substituted material can be attributed to the fact that these states hybridize strongly with the Fe bands and are distributed over essentially the same energy region.

The above results are in good agreement with previous reports, where similar trends have also been extracted.[4,13,14] An important new observation here is that replacing Fe by heavier Ni and Cu removes Fe states close to the Fermi level and adds impurity states at higher binding energy, as is nicely demonstrated by the data in Fig. 1. The PES data thereby shows that the heavier TMs contribute less to the states close to the Fermi level. Note that these data can only provide qualitative information about changes in the density of states (DOS), because the PES cross sections for Fe, Co, Ni, and Cu are different and not known precisely.

Resonant PES data for the three substituted samples are presented in Fig. 2, including the XAS and the non-resonant PES. The intensity maps as a function of photon energy ($h\nu$) and binding energy (ϵ_B) have been obtained by subtracting the nonresonant PES spectrum, in order to highlight the resonant features. In all cases a strong increase of the PES intensity can be observed, as soon as the photon energy is tuned to the TM-impurity L_3 edge. The PES maps in Fig. 2 show the typical Auger features of resonant PES, namely (i) a resonant Raman Auger decay right at the TM L_3 threshold, which occurs at a fixed binding energy, and (ii) the conventional Auger decay at higher $h\nu$, which leads to a constant kinetic energy of the emitted Auger electron ($\epsilon_{\mathrm{kin}}^{\mathrm{AES}}$) and therefore shifts linearly when plotted as a function of $\epsilon_B = h\nu - \epsilon_{\mathrm{kin}}^{\mathrm{AES}}$.[23,24] Comparing the PES maps for Co, Ni, and Cu, it can immediately be observed that the Auger final states move to higher binding energies with increasing *Z* and, at the same time, develop a clear fine structure.

We will consider the following processes: $3d^n + h\nu \rightarrow \underline{2p}3d^n + e^* \rightarrow 3d^{n-2} + k + e^*$, with $\underline{2p}$ the $2p$ core hole, e^* the corresponding photoexcited electron, and k the emitted Auger electron. The first step corresponds to the absorption of the incoming photon and the second step is the LVV Auger decay. Note that e^* does not participate in the LVV Auger decay, resulting in two additional holes in the 3*d* valence shell. In the case of an isolated atom, the interaction between the two holes in the valence shell splits the Auger final state into a characteristic multiplet, consisting of different terms with different energy, total spin *S*, and angular momentum *L*. Each of these final LS terms gives rise to a line in the total spectrum with a specific intensity. If these lines are sharp and well defined, the multiplet structure of the AES provides a unique fingerprint of the electronic final state configuration.

The broad AES spectrum of Co, however, does not show any clear multiplet structure, as can be observed in Figs. 2(a) and 2(d). This implies that the Co states are strongly hybridized with the Fe host: the state with the two holes on Co couples strongly to the continuum of states where one hole has moved from Co into the Fe host, resulting in the observed broad and structureless spectrum. This observation is in agreement with a recent resonant PES study on $Ca(Fe_{1-x}Co_x)_2As_2$.[24]

As can be seen in Figs. 2(b) and 2(e), Ni shows a much more structured LVV spectrum. The observed lineshape is essentially identical to that found for Ni metal,[17,21] showing structures that agree very well with an atomic Ni:$3d^8$ Auger final state multiplet. Both the energy splitting between the different terms and the relative intensities obtained by the

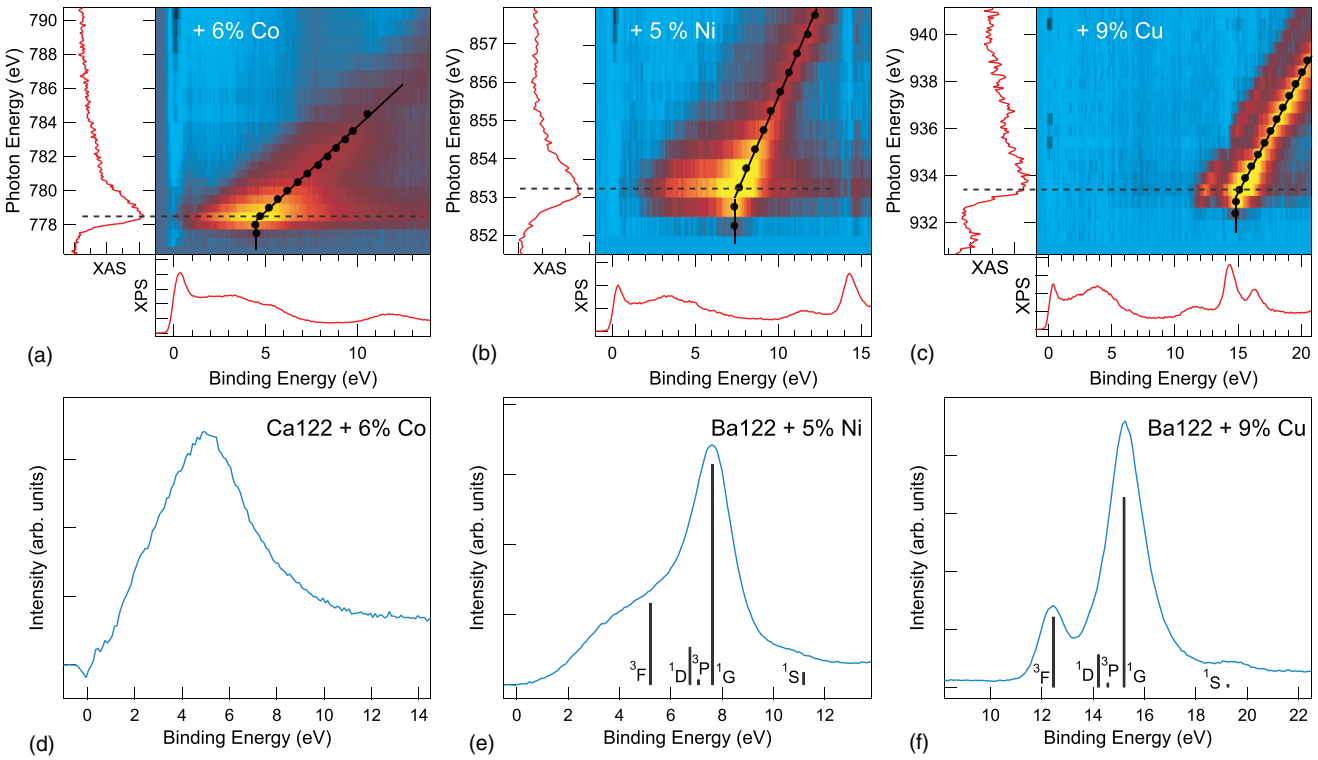

FIG. 2. (Color online) Resonant PES scans across the L_3 edge for (a) $Ca(Fe,Co)_2As_2$, (b) $Ba(Fe,Ni)_2As_2$, and (c) $Ba(Fe,Cu)_2As_2$. On the left side of each map in the top row the XAS spectra are displayed. From each map an off-resonance PES spectra was subtracted, which is shown below each map. The AES peak for each incident photon energy is indicated by black dots, showing the crossover from a resonant Raman ($\epsilon_B = \text{const}$) to the normal AES decay ($\epsilon_K = \text{const}$). The lower panels show LVV Auger spectra corresponding to the cuts indicated by the dashed lines in the upper panels. Term splittings of the atomic $3d^8$ final state were calculated using Cowan's code (Ref. 20) and the AES intensities were taken from Refs. 21 and 22 (vertical lines). The calculations do not take into account the full resonance process, but consider the Auger decay of the core hole state only.

atomic calculation[21] are in very good agreement with the experimental data.

The observation of a $3d^8$ Auger final state for Ni is remarkable, because it is incompatible with the often assumed electron doping. The latter would result in a Ni:$3d^6$ in the ground state, from which the $3d^8$ Auger final state cannot be reached at all. A Ni:$3d^6$ is hence excluded by our data. Instead, the data implies a strong Ni:$3d^9$ component in the ground state. Here the $3d^8$ final state can be reached via $3d^9 + h\nu \rightarrow \underline{2p}\, 3d^{10}(\text{screening}) + e^* \rightarrow 3d^8 + e^* + k$, where the $3d^{10}$ in the intermediate state is due to the screening of the core hole. In principle, a Ni:$3d^{10}$ component of the ground state would also be possible. But we can exclude this possibility based on the XAS data, where we and others[4] observe a strong XAS peak at the Ni L_3 edge, which would be absent for a $3d^{10}$ configuration of Ni.

The LVV spectrum for Cu is even more structured, as demonstrated in Figs. 2(c) and 2(f). Again, we compare the experimental results to an atomic multiplet calculation[22] and find excellent agreement with a Cu:$3d^8$ final state multiplet. This identification is further supported by comparing our data to previously published results on Cu metal and CuO_2, which also show the Cu:$3d^8$ final state multiplet.[25,26]

The Cu AES data therefore unambiguously identify a significant Cu:$3d^{10}$ or Cu:$3d^9$ component in the ground state. In fact, since the XAS shown in Fig. 2(c) agrees very well with what is expected for a Cu:$3d^{10}$,[27] we can exclude a significant population of Cu:$3d^9$. This result is also in accord with the high $\langle \epsilon_B^{\text{Cu}} \rangle$ of the Cu:$3d$ states determined by the PES data in Fig. 1. A Cu:$3d^{10}$ state was also deduced in a recent x-ray spectroscopy study[4] and indirectly concluded from macroscopic measurements on $BaCu_2As_2$.[28] We can therefore safely conclude that Cu is predominantly in a Cu:$3d^{10}$ configuration, i.e., the Cu-impurities have a closed shell.

In the current situation, a realistic estimate can be made for the effective onsite Coulomb interaction U_{eff} on the impurities, using the Cini-Sawatzky (CS) theory.[29–31] Within this approach the AES intensity is

$$I(\epsilon) = \frac{D(\epsilon)}{[1 - U_{\text{eff}} F(\epsilon)]^2 + [\pi\, U_{\text{eff}}\, D(\epsilon)]^2},$$

where ϵ is the energy of the two-hole Auger final state relative to the chemical potential, $D(\epsilon) = \int \rho(x)\, \rho(\epsilon - x) dx$, $F(\epsilon) = P \int D(x)/(\epsilon - x) dx$, and ρ is the impurity DOS with the occupied part normalized to 1. Here, we determined ρ by means of density functional theory. These band structure calculations were done in the local density approximation using the full potential code WIEN2K,[32] as described in Ref. 13. The results of this calculation for noninteracting [$U_{\text{eff}} = 0$, $I(\epsilon) = D(\epsilon)$] and interacting ($U_{\text{eff}} \neq 0$) holes are presented in Fig. 3.

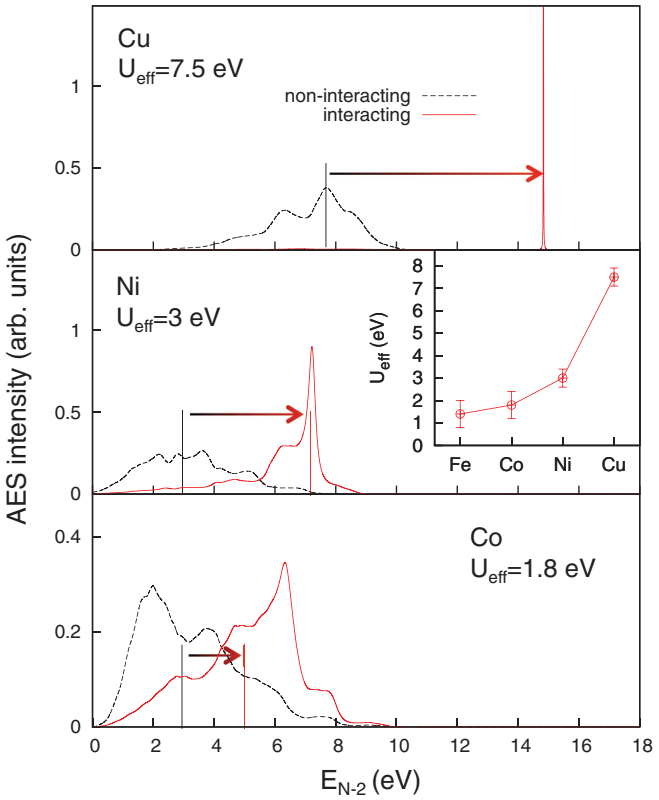

FIG. 3. (Color online) Simulated AES spectra and estimated U_{eff}. ϵ on the binding energy scale is denoted as E_{N-2}. Noninteracting case: The continuum described by D shifts to higher energies with increasing Z due to the increased binding energy of the impurity states. Interacting case: While no two-hole bound state is formed for Co, the U_{eff} is large enough to push a two-hole bond state out of the D continuum.

The energies of the Auger final states on the binding energy scale were determined using the resonant Auger Raman spectra. For Fe (not shown) and Co we determined U_{eff} by fitting the center of mass of the calculated spectra to the corresponding experimental values, which are (4.0 ± 0.5) eV for Fe and (4.5 ± 0.5) eV for Co. For Ni and Cu, we set U_{eff} so as to match the measured binding energies of the ^1G term, which are 7.35 and 14.85 eV, respectively.

In this way we obtain $U_{\text{eff}} = (1.4 \pm 0.6)$ eV, (1.8 ± 0.6) eV, (3.0 ± 0.4) eV, and (7.5 ± 0.4) eV for Fe, Co, Ni, and Cu (inset of Fig. 3). U_{eff}-values for Fe and Co were also reported previously[19,24,31] and are in fair agreement with our results. The analysis explains the development of the quasiatomic LVV: with increasing U_{eff} the Auger final states are pushed out of the continuum of states given by $D(\epsilon)$ and form localized bound states.[29] The emerging multiplet structure with increasing Z in Fig. 2 is therefore a direct consequence of the increasing U_{eff}.

The U_{eff} determined here corresponds to the effective Coulomb interaction between two holes in the valence shell. U_{eff} depends on the spatial structure of the two-hole wave function and, most importantly, the screening of these holes by the surrounding charges. Note also that the increase of U_{eff} with Z is consistent with the observed charge accumulation, i.e., the filling of the TM:3d-shell with increasing Z, as this indeed reduces the number of possible screening channels and thereby results in a larger effective onsite Coulomb repulsion (cf. Ref. 33).[34]

IV. DISCUSSION AND CONCLUSION

Our data confirm the strong overlap and hybridization of the Co and Fe states. The Co states therefore have a significant Fe:3d character, which is consistent with the observed electron doping of the Fe bands.[6–8,14] But in addition to this, scattering centers are also created within the FeAs layers, with a scattering potential that is given by $\langle\epsilon_B^{\text{Co}}\rangle - \langle\epsilon_B^{\text{Fe}}\rangle \simeq 0.3$ eV ($\langle\epsilon_B^{\text{Fe}}\rangle = 0.4$ eV[24]) and $U_{\text{eff}}^{\text{Co}} - U_{\text{eff}}^{\text{Fe}} \simeq 0.4$ eV. Please note that not only the different binding energy, but also the different onsite Coulomb repulsion on the TM-impurity is related to changes in the electronic structure of the substituted material.

The Ni states are located close to the bottom of the Fe bands, and the data in Fig. 1 show that these impurity states contribute much less to the states close to the Fermi level than the Co-impurity states. At the same time, the Ni:3d^9 observed here is direct and clear experimental proof for the charge accumulation at Ni. The scattering potential due to the Ni impurities is much more severe than in the Co case, because $\langle\epsilon_B^{\text{Ni}}\rangle - \langle\epsilon_B^{\text{Fe}}\rangle \simeq 1$ eV and $U_{\text{eff}}^{\text{Ni}} - U_{\text{eff}}^{\text{Fe}} \simeq 1.6$ eV. These energies are already comparable to the band width $W \simeq 2$ eV of the occupied Fe:3d-states, i.e., the impurity scattering is significant.

The Cu impurities differ from the two previous cases in that they form bound states well below the Fe bands with little Fe:3d character. The observed Cu:3d^{10} configuration implies a strong charge accumulation at Cu. We also find that the scattering due to Cu with its closed shell is very strong ($\langle\epsilon_B^{\text{Cu}}\rangle - \langle\epsilon_B^{\text{Fe}}\rangle \simeq 3.6$ eV, $U_{\text{eff}}^{\text{Cu}} - U_{\text{eff}}^{\text{Fe}} \simeq 6.1$ eV). Correspondingly, a few percent Cu substitution will already make the definition of a FS difficult. We note that the above is in line with a recent neutron scattering study.[35]

To our knowledge, the present AES data is the first direct experimental observation of the charge accumulation at TM impurities in the iron pnictides. Although this accumulation is only resolved here for Ni and Cu, it is also expected for Co on theoretical grounds.[3,13,24] The charge accumulation at the TM impurities is important, as it enables us to reconcile the conflicting results coming from momentum-resolved photoemission and local probes such as x-ray absorption and Moessbauer spectroscopy: even though charge carriers can be added to the Fe:3d bands via TM substitution, as shown by angle-resolved photoemission, the delocalized charge carriers have an increased probability of being around the heavier TM substitute due to the additional impurity potential. Charge density therefore piles up around the TM, resulting in an essentially constant 3d-electron count at Fe, as was indeed observed by local probes.[9–11]

Our experiments do not enable us to observe the filling of the Fe:3d bands directly. However, the PES data in Fig. 1 together with the observed Cu:3d^{10} further imply that the charge accumulation increases in going from Co over Ni to Cu. Taken together our results strongly support the notion that the larger the Z of the substituted TM = Co, Ni, or Cu, the smaller is the amount of charge added to the Fe:3d bands and the bigger is the effect of the impurity scattering.

If and how many electrons the TM substitution adds to the Fe bands should therefore depend crucially on the impurity-host hybridization and the energy difference between the host and impurity states, as was also recently deduced by Ideta *et al.* based on angle-resolved photoemission experiments.[14] These parameters depend on the chosen TM and their effects go beyond a mere charge carrier doping and rigid band models. Especially the additional scattering potentials, which are quantified here, affect the low-energy electronic structure, play a role for the phase diagrams, and need to be considered in realistic theoretical models. Interestingly, even though the maximum critical superconducting temperature reached via Ni substitution is somewhat reduced as compared to the Co substituted materials, the occurrence of HTS in these systems shows nevertheless that the superconductivity in the iron pnictides is rather robust against impurity scattering.

ACKNOWLEDGMENTS

Work at the IFW was supported by the DFG (Grants No. BE1749/13 and No. SPP1458). S.W., J.G., and R.K. acknowledge support by the DFG through the Emmy-Noether program (Grants No. WU595/3-1 and No. GE1647/2-1). V.B. acknowledges financial support by the DAAD, and G.L., I.S.E., and G.A.S. from the Canadian funding agencies NSEC, SFI, and CRC. We thank HZB for the allocation of synchrotron radiation beamtime and S. Krause, M. Oehzelt and S. Pohl for their support at the beamline.

APPENDIX: SAMPLE GROWTH AND CHARACTERIZATION

All $Ba(Fe_{1-x}TM_x)_2As_2$ crystals used for the present study were grown by the self-flux technique as described in Ref. 16, using FeAs as flux. In case of the $Ba(Fe_{1-x}Co_x)_2As_2$ system, details about the crystal growth, the characterization and the physical properties were published in Ref. 16. Here we provide additional details regarding the growth and the characterization of the Ni and Cu substituted $BaFe_2As_2$ single crystals. The prereacted precursor materials FeAs, Fe_2As, BaAs, and metallic Ni or Cu (TM) were mixed, leading to a $Ba(Fe_{1-x}TM_x)_{3.1}As_{3.1}$ composition. This composition was used to achieve a homogeneous melt at $T = 1463$ K. The melt was cooled slowly under a temperature gradient in a double-wall crucible assembly to obtain large and flux-free single crystals of $Ba(Fe_{1-x}Ni_x)_2As_2$ and $Ba(Fe_{1-x}Cu_x)_2As_2$. Two examples for the obtained single crystals with typical dimensions are shown in the Fig. 4. The $Ca(Fe_{1-x}Co_x)_2As_2$ crystals were grown from Sn flux as described in Ref. 15, where the characterization of these samples is reported as well.

The high quality of the grown single crystals was assured by several complementary techniques. From each batch, several samples were examined with a scanning electron microscope (SEM, Philips XL 30) equipped with an electron microprobe analyzer for the semi-quantitative elemental analysis in the energy dispersive x-ray (EDX) mode. Using EDX, the Ni and Cu concentrations were determined by averaging over several different points on the sample surface. The estimated composition from the EDX for the present single crystals is $Ba(Fe_{0.95}Ni_{0.05})_2As_2$ and $Ba(Fe_{0.91}Cu_{0.09})_2As_2$. In general, the

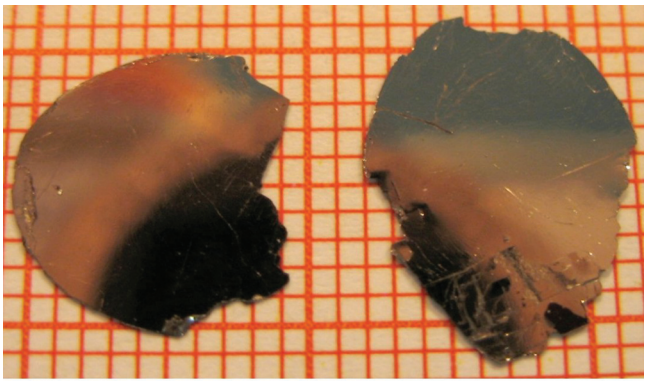

FIG. 4. (Color online) As grown $Ba(Fe_{0.95}Ni_{0.05})_2As_2$ single crystals.

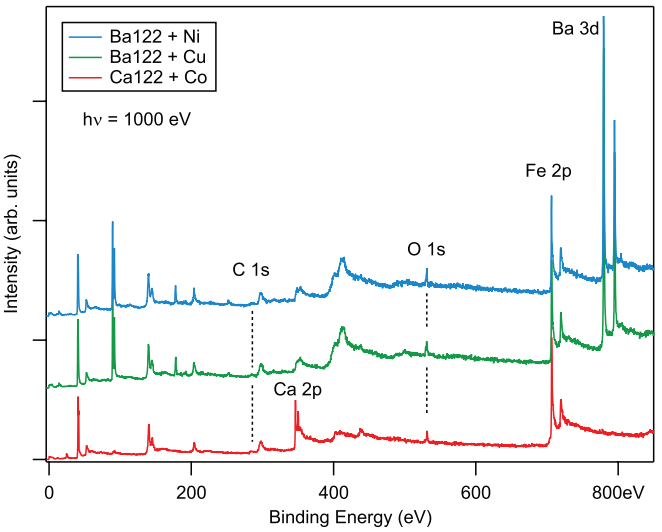

FIG. 5. (Color online) XPS survey scans. Only a small trace of oxygen is observed, which can at least partially be attributed to adsorbates on the sample surface and verifies the high purity of our samples.

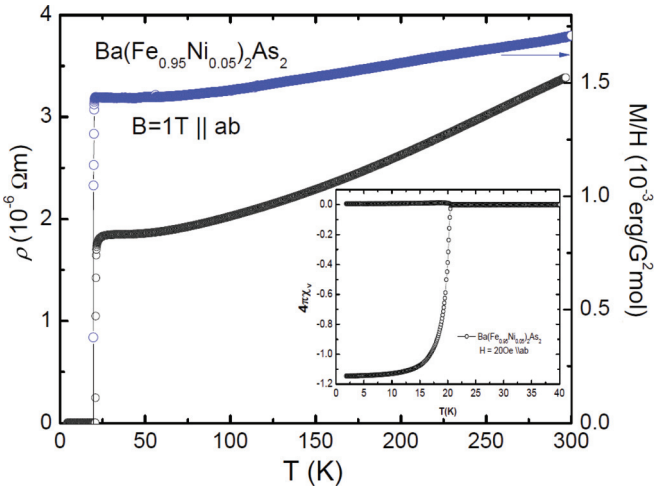

FIG. 6. (Color online) Magnetization and resistivity measurement of $Ba(Fe_{0.95}Ni_{0.05})_2As_2$ single crystals.

error of an EDX analysis is about 2 mass percent without any additional standardization procedure. However, the method of averaging reduces the size of the error bars significantly. In this way the concentration x of Co, Ni, and Cu was determined to be (0.06 ± 0.01), (0.05 ± 0.01), and (0.09 ± 0.01).

In addition to this, the TM contents of the studied samples were also supported by our *in situ* by PES measurements. The *in situ* XPS measurements also do not show any sign of a significant oxygen contamination in any of the studied samples. Representative XPS survey scans are displayed in Fig. 5. The weak O 1*s* line is comparable to what has been reported previously in the literature for high-purity samples,[4] which verifies the high quality of the studied single crystals. Our XAS measurements also exclude the presence of Fe-oxide impurities, which would leave a clear fingerprint in these spectra.[10]

Prior the synchrotron experiments, the high quality of our single crystals was also checked by XRD, resistivity, and magnetization measurements. In Fig. 6 we show representative measurements for our $Ba(Fe_{0.95}Ni_{0.05})_2As_2$ single crystals. The data in Fig. 6 reveal that the structural and magnetic transitions are completely suppressed by 5% Ni substitution, whereas bulk superconductivity occurs. This is in excellent agreement with the literature.[36] Furthermore, the superconducting transition at $T_C = 21$ K is very sharp and, within the error bars of our experiment, we find a superconducting volume fraction of 100%. This further confirms the very high quality of our single crystals. Also the Cu-substituted samples were characterized by the same methods prior the synchrotron experiments. The structural quality was verified by XRD and, in agreement with the previous literature, the sample with 9% Cu substitution does not show superconductivity down to 1.8 K.

*j.geck@ifw-dresden.de

[1] G. R. Stewart, Rev. Mod. Phys. **83**, 1589 (2011).

[2] A. S. Sefat, R. Jin, M. A. McGuire, B. C. Sales, D. J. Singh, and D. Mandrus, Phys. Rev. Lett. **101**, 117004 (2008).

[3] T. Berlijn, C.-H. Lin, W. Garber, and W. Ku, Phys. Rev. Lett. **108**, 207003 (2012).

[4] J. A. McLeod, A. Buling, R. J. Green, T. D. Boyko, N. A. Skorikov, E. Z. Kurmaev, M. Neumann, L. D. Finkelstein, N. Ni, A. Thaler, S. L. Budko, P. C. Canfield, and A. Moewes, J. Phys.: Condens. Matter **24**, 215501 (2012).

[5] P. C. Canfield and S. L. Bud'ko, Annu. Rev. Condens. Matter Phys. **1**, 27 (2010).

[6] C. Liu, A. D. Palczewski, R. S. Dhaka, T. Kondo, R. M. Fernandes, E. D. Mun, H. Hodovanets, A. N. Thaler, J. Schmalian, S. L. Bud'ko, P. C. Canfield, and A. Kaminski, Phys. Rev. B **84**, 020509 (2011).

[7] W. Malaeb, T. Yoshida, A. Fujimori, M. Kubota, K. Ono, K. Kihou, P. M. Shirage, H. Kito, A. Iyo, H. Eisaki, Y. Nakajima, T. Tamegai, and R. Arita, J. Phys. Soc. Jpn. **78**, 123706 (2009).

[8] S. Konbu, K. Nakamura, H. Ikeda, and R. Arita, J. Phys. Soc. Jpn. **80**, 123701 (2011).

[9] E. M. Bittar, C. Adriano, T. M. Garitezi, P. F. S. Rosa, L. Mendonça-Ferreira, F. Garcia, G. d. M. Azevedo, P. G. Pagliuso, and E. Granado, Phys. Rev. Lett. **107**, 267402 (2011).

[10] M. Merz, F. Eilers, T. Wolf, P. Nagel, H. v. Löhneysen, and S. Schuppler, Phys. Rev. B **86**, 104503 (2012).

[11] A. Khasanov, S. C. Bhargava, J. G. Stevens, J. Jiang, J. D. Weiss, E. E. Hellstrom, and A. Nath, J. Phys.: Condens. Matter **23**, 202201 (2011).

[12] M. W. Haverkort, I. S. Elfimov, and G. A. Sawatzky, arXiv:1109.4036.

[13] H. Wadati, I. Elfimov, and G. A. Sawatzky, Phys. Rev. Lett. **105**, 157004 (2010).

[14] S. Ideta, T. Yoshida, I. Nishi, A. Fujimori, Y. Kotani, K. Ono, Y. Nakashima, S. Yamaichi, T. Sasagawa, M. Nakajima, K. Kihou, Y. Tomioka, C. H. Lee, A. Iyo, H. Eisaki, T. Ito, S. Uchida, and R. Arita, Phys. Rev. Lett. **110**, 107007 (2013).

[15] L. Harnagea, S. Singh, G. Friemel, N. Leps, D. Bombor, M. Abdel-Hafiez, A. U. B. Wolter, C. Hess, R. Klingeler, G. Behr, S. Wurmehl, and B. Büchner, Phys. Rev. B **83**, 094523 (2011).

[16] S. Aswartham, C. Nacke, G. Friemel, N. Leps, S. Wurmehl, N. Wizent, C. Hess, R. Klingeler, G. Behr, S. Singh, and B. Büchner, J. Cryst. Growth **314**, 341 (2011).

[17] M. Weinelt, A. Nilsson, M. Magnuson, T. Wiell, N. Wassdahl, O. Karis, A. Föhlisch, N. Mårtensson, J. Stöhr, and M. Samant, Phys. Rev. Lett. **78**, 967 (1997).

[18] S. de Jong, Y. Huang, R. Huisman, F. Massee, S. Thirupathaiah, M. Gorgoi, F. Schaefers, R. Follath, J. B. Goedkoop, and M. S. Golden, Phys. Rev. B **79**, 115125 (2009).

[19] A. Koitzsch, R. Kraus, T. Kroll, M. Knupfer, B. Büchner, H. Eschrig, D. R. Batchelor, G. L. Sun, D. L. Sun, and C. T. Lin, Phys. Rev. B **81**, 174519 (2010).

[20] R. D. Cowan, *The Theory of Atomic Structure and Spectra* (University of California Press, Berkeley, 1981).

[21] P. A. Bennett, J. C. Fuggle, F. U. Hillebrecht, A. Lenselink, and G. A. Sawatzky, Phys. Rev. B **27**, 2194 (1983).

[22] E. J. McGuire, Phys. Rev. A **16**, 2365 (1977).

[23] F. Gel'mukhanov and H. Ågren, Phys. Rep. **312**, 87 (1999).

[24] G. Levy, R. Sutarto, D. Chevrier, T. Regier, R. Blyth, J. Geck, S. Wurmehl, L. Harnagea, H. Wadati, T. Mizokawa, I. S. Elfimov, A. Damascelli, and G. A. Sawatzky, Phys. Rev. Lett. **109**, 077001 (2012).

[25] A. Föhlisch, O. Karis, M. Weinelt, J. Hasselström, A. Nilsson, and N. Mårtensson, Phys. Rev. Lett. **88**, 027601 (2001).

[26] L. H. Tjeng, C. T. Chen, J. Ghijsen, P. Rudolf, and F. Sette, Phys. Rev. Lett. **67**, 501 (1991).

[27] M. Grioni, J. F. van Acker, M. T. Czyżyk, and J. C. Fuggle, Phys. Rev. B **45**, 3309 (1992).

[28] V. K. Anand, P. K. Perera, A. Pandey, R. J. Goetsch, A. Kreyssig, and D. C. Johnston, Phys. Rev. B **85**, 214523 (2012).

[29] G. A. Sawatzky, Phys. Rev. Lett. **39**, 504 (1977).

[30] M. Vos, D. v. d. Marel, and G. A. Sawatzky, Phys. Rev. B **29**, 3073 (1984).

[31] P. Vilmercati, C. P. Cheney, F. Bondino, E. Magnano, M. Malvestuto, M. A. McGuire, A. S. Sefat, B. C. Sales, D. Mandrus, D. J. Singh, M. D. Johannes, and N. Mannella, Phys. Rev. B **85**, 235133 (2012).

[32]P. Blaha, K. Schwarz, G. Madsen, D. Kvasnicka, and J. Luitz, *WIEN2k: An Augmented Plane Wave Plus Local Orbitals Program for Calculating Crystal Properties* (TU Wien, Austria, 2001).

[33]I. Leonov, A. N. Yaresko, V. N. Antonov, U. Schwingenschlögl, V. Eyert, and V. I. Anisimov, J. Phys.: Condens. Matter **18**, 10955 (2006).

[34]Screening strongly reduces the bare (atomic) Coulomb repulsion of $\sim$25 $+$eV to the observed U_{eff}. Note that the onsite repulsion parameter U used in various theories is model dependent, because different approximations for the wave functions are used and the screening is taken into account to different degrees.

[35]M. G. Kim, J. Lamsal, T. W. Heitmann, G. S. Tucker, D. K. Pratt, S. N. Khan, Y. B. Lee, A. Alam, A. Thaler, N. Ni, S. Ran, S. L. Bud'ko, K. J. Marty, M. D. Lumsden, P. C. Canfield, B. N. Harmon, D. D. Johnson, A. Kreyssig, R. J. McQueeney, and A. I. Goldman, Phys. Rev. Lett. **109**, 167003 (2012).

[36]S. L. Bud'ko, N. Ni, and P. C. Canfield, Phys. Rev. B **79**, 220516(R) (2009).